

$\Lambda_c N$ interaction in leading order covariant chiral effective field theory

Jing Song,¹ Yang Xiao,^{1,2} Zhi-Wei Liu,¹ Chun-Xuan Wang,¹ Kai-Wen Li,^{3,1,*} and Li-Sheng Geng^{1,3,4,5,†}

¹*School of Physics, Beihang University, Beijing, 102206, China*

²*Université Paris-Saclay, CNRS/IN2P3, IJCLab, Orsay, 91405, France*

³*Beijing Advanced Innovation Center for Big Data-Based Precision Medicine,
School of Medicine and Engineering, Beihang University,*

Key Laboratory of Big Data-Based Precision Medicine (Beihang University),

Ministry of Industry and Information Technology, Beijing, 100191, China

⁴*Beijing Key Laboratory of Advanced Nuclear Materials and Physics, Beihang University, Beijing, 102206, China*

⁵*School of Physics and Microelectronics, Zhengzhou University, Zhengzhou, Henan, 450001, China*

(■Dated: October 15, 2020)

We study the $\Lambda_c N$ interaction in the covariant chiral effective field theory (ChEFT) at leading order. All the relevant low-energy constants are determined by fitting to the lattice QCD simulations from the HAL QCD Collaboration. Extrapolating the results to the physical point, we show that the $\Lambda_c N$ interaction is weakly attractive in the 1S_0 channel, but in the 3S_1 channel, it is only attractive at extremely low energies and soon turns repulsive for larger laboratory energy. Furthermore, we show that the neglect of the $^3S_1 - ^3D_1$ coupling provided by the leading order covariant ChEFT would result in an attractive interaction in the 3S_1 channel at the physical point, which coincides with the previous non-relativistic ChEFT study. As a byproduct, we predict the 3D_1 phase shifts and the mixing angle ε_1 , which can be checked by future lattice QCD simulations. In addition, we compare the $\Lambda_c N$ interaction with the ΛN and NN interactions to study how the baryon-nucleon (BN) interactions evolve as a function of the baryon mass with the replacement of a light quark by a strange or charm quark in the baryon (B).

PACS numbers: 13.75.Ev, 12.39.Fe, 21.30.Fe

I. INTRODUCTION

Baryon-baryon (BB) interactions are one of the most important inputs in studies of hadronic matter. At present, the low energy nucleon-nucleon (NN) interaction has already been comprehensively studied both phenomenologically and model independently [1–5]. The investigation of the hyperon-nucleon (YN) interaction has achieved significant success as well [6–11]. Hypernuclear spectroscopy provides one of the most important sources from which YN and hyperon-hyperon (YY) interactions can be derived. As a natural extension of NN and YN interactions, the charmed hyperon-nucleon ($Y_c N$) interaction, has also been studied with growing interests [12–19]. High energy facilities such as BEPC in China [20, 21], J-PARC in Japan [22], and FAIR in Germany [23] all have ongoing/proposed experiments on charm physics, for instance the production of Λ_c and Σ_c hyperons and their interactions with other hadrons [24].

Early theoretical studies, based on either meson-exchange models [12–17] or constituent quark models [18, 19], indicated that the $Y_c N$ ($Y_c = \Lambda_c, \Sigma_c$) interaction is fairly attractive. Particularly, compared with the ΛN interaction, the strange meson (K, K^*) exchanges are replaced by the charmed meson (D, D^*) exchanges in the $\Lambda_c N$ interaction [13, 14, 16] in meson-exchanged models. This would result in less (more) attraction in the S - (P -) partial waves in the $\Lambda_c N$ interaction than in the corresponding ΛN potential, because of the larger masses of exchanged mesons.

Recently, the HAL QCD Collaboration has performed lattice QCD simulations for unphysical pion masses to study the $\Lambda_c N$ interaction [25]. They obtained the S -wave phase shifts for $m_\pi = 410$ MeV, 570 MeV, and 700 MeV. These results were subsequently studied in the next-to-leading order non-relativistic chiral effective field theory (ChEFT) and extrapolated to the physical point and a moderately attractive $\Lambda_c N$ interaction was found for both the 1S_0 and 3S_1 channels [26]. In a later work, the S -wave $\Sigma_c N$ interaction with isospin 1/2 was studied by the HAL QCD Collaboration as well [27]. Taking these results as inputs, Meng et al. [28] calculated the $\Sigma_c N$ interaction to the next-to-leading order in the non-relativistic ChEFT and found that the 3S_1 interaction for isospin 1/2 is weakly attractive, but the interaction for isospin 3/2 is strongly attractive, resulting in a $\Sigma_c N$ bound state. It should be stressed that the latter prediction depends on the quark model inputs adopted.

As all the lattice QCD simulations of the $Y_c N$ system were still performed for unphysical light quark (pion) masses, a reliable extrapolation of these results to the physical point is essential to guide future experiments and to gain insights on the $Y_c N$

*E-mail me at: kaiwen.li@buaa.edu.cn

†E-mail me at: lisheng.geng@buaa.edu.cn

interaction. In a series of recent works, we have shown that the recently proposed covariant ChEFT approach can be used for such a purpose. In Refs. [29–32], it was shown that the strangeness $S = -1$ lattice QCD YN interaction can be described reasonably well, so is the strangeness $S = -2$ YN/YY interaction. The extrapolated results are also consistent with limited experimental data. In a more recent work [33], we showed that the lattice QCD NN phase shifts for the 1S_0 and $^3S_1 - ^3D_1$ partial waves can be simultaneously described together with their physical counterparts by the leading order (LO) covariant ChEFT, implying that a reliable chiral extrapolation of lattice QCD results for unphysical pions masses smaller than 500 MeV is possible. An interesting discovery of Ref. [33] is that the $^3S_1 - ^3D_1$ coupled channel is described by the same two low-energy constants (LECs), thus allowing one to make predictions for the 3D_1 phase shifts and the mixing angle ε_1 using only the 3S_1 phase shifts as inputs.

In this work, we revisit the HAL QCD results [25] in the covariant ChEFT at leading order. Our purpose is threefold. First, we provide an independent extrapolation of the HAL QCD results, in addition to that of Ref. [26]. Second, we predict the 3D_1 phase shifts and the mixing angle ε_1 , so that they can be checked by future lattice QCD simulations, which could also provide a non-trivial check of the covariant ChEFT. Third, we investigate the quark mass dependence of baryon-nucleon interactions by comparing those of NN , ΛN , and $\Lambda_c N$.

This paper is organized as follows. In Sec. II, we briefly introduce the covariant ChEFT for the $Y_c N$ system, including covariant chiral Lagrangians, potentials, and the scattering equation, as well as our strategy to determine the unknown LECs. In Sec. III we show the fitted results and extrapolations, and discuss about coupled channel effects and quark mass dependence in the NN , ΛN , and $\Lambda_c N$ interactions. Followed by a short summary and outlook in Sec. IV.

II. LEADING ORDER COVARIANT CHIRAL EFFECTIVE FIELD THEORY

In this section, we briefly introduce the covariant ChEFT for the $Y_c N$ interaction. At leading order, the $Y_c N$ potentials consist of contributions from non-derivative four-baryon contact terms (CT) and one-meson-exchanges (OME), as shown in Fig. 1.

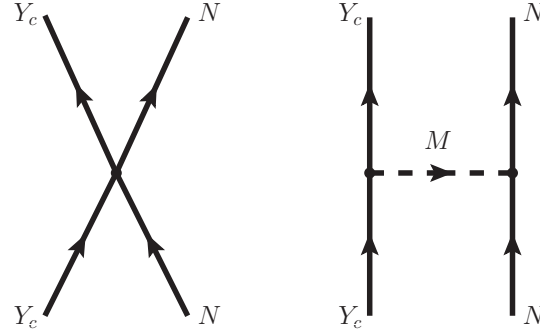


FIG. 1: Leading order Feynman diagrams for non-derivative four-baryon contact terms and one-meson-exchanges.

The LO Lagrangian for the contact terms is:

$$\mathcal{L}_{\text{CT}}^{Y_c N \rightarrow Y_c N} = C_i (\bar{Y}_c \Gamma_i Y_c) (\bar{N} \Gamma_i N), \quad (1)$$

where C_i ($i = 1 \dots 5$) are the LECs that need to be determined by fitting to either experimental or lattice QCD data, and Γ_i ($i = 1 \dots 5$) are the elements of the Clifford algebra,

$$\Gamma_1 = 1, \quad \Gamma_2 = \gamma^\mu, \quad \Gamma_3 = \sigma^{\mu\nu}, \quad \Gamma_4 = \gamma^\mu \gamma_5, \quad \Gamma_5 = \gamma_5.$$

Then potentials are derived with the full baryon spinor,

$$u_B(p, s) = N_p \left(\frac{1}{E_p + M_B} \right) \chi_s, \quad N_p = \sqrt{\frac{E_p + M_B}{2M_B}}, \quad (2)$$

where $E_p = \sqrt{p^2 + M_B^2}$, and $M_B = M_{Y_c}$ or M_N the mass of charmed baryon or nucleon. By performing partial wave

projection, the 1S_0 and $^3S_1 - ^3D_1$ CT potentials in the LSJ basis read

$$V_{1S_0}^{Y_c N} = \xi_{Y_c N} \left[C_{1S_0} \left(R_{p'}^N R_{p'}^{Y_c} + R_p^N R_p^{Y_c} \right) + C'_{1S_0} \left(R_{p'}^N R_p^N R_{p'}^{Y_c} R_p^{Y_c} + 1 \right) \right], \quad (3)$$

$$V_{3S_1}^{Y_c N} = \frac{1}{9} \xi_{Y_c N} \left\{ 2 \left(C_{1S_0} - C'_{1S_0} \right) \left(R_{p'}^{Y_c} R_p^{Y_c} - R_p^N R_p^N \right) \right. \\ \left. + C_{3S_1} \left(-6 R_{p'}^N R_p^N + 9 R_{p'}^N R_{p'}^{Y_c} + 9 R_p^N R_p^{Y_c} + 6 R_{p'}^{Y_c} R_p^{Y_c} \right) \right. \\ \left. + 9 C'_{3S_1} \left[R_{p'}^{Y_c} R_p^{Y_c} \left(R_p^N R_p^N - 2 \right) + 2 R_{p'}^N R_p^N + 9 \right] \right\}, \quad (4)$$

$$V_{3D_1-3S_1}^{Y_c N} = \frac{\xi_{Y_c N}}{9\sqrt{2}} \left\{ \left(C_{1S_0} - C'_{1S_0} \right) \left[R_p^N \left(R_{p'}^N + 3 R_{p'}^{Y_c} \right) - R_p^{Y_c} \left(3 R_{p'}^N + R_{p'}^{Y_c} \right) \right] \right. \\ \left. + C_{3S_1} \left[9 R_p^{Y_c} \left(R_{p'}^N + 4 R_p^N \right) + 3 R_{p'}^N R_p^N - 3 R_{p'}^{Y_c} \left(3 R_p^N + R_p^{Y_c} \right) \right] \right. \\ \left. + 9 C'_{3S_1} \left\{ R_{p'}^{Y_c} \left[R_p^N \left(4 R_{p'}^N R_p^{Y_c} + 3 \right) + R_p^{Y_c} \right] - R_p^N \left(R_p^N + 3 R_p^{Y_c} \right) \right\} \right\}, \quad (5)$$

$$V_{3S_1-3D_1}^{Y_c N} = \frac{\xi_{Y_c N}}{9\sqrt{2}} \left\{ \left(C_{1S_0} - C'_{1S_0} \right) \left[R_{p'}^N \left(R_p^N + 3 R_p^{Y_c} \right) - R_{p'}^{Y_c} \left(3 R_p^N + R_p^{Y_c} \right) \right] \right. \\ \left. + C_{3S_1} \left[9 R_{p'}^{Y_c} \left(R_p^N + 4 R_{p'}^N \right) + 3 R_p^N R_{p'}^N - 3 R_p^{Y_c} \left(3 R_{p'}^N + R_{p'}^{Y_c} \right) \right] \right. \\ \left. + 9 C'_{3S_1} \left\{ R_{p'}^{Y_c} \left[R_{p'}^N \left(4 R_p^N R_{p'}^{Y_c} + 3 \right) + R_p^{Y_c} \right] - R_p^N \left(R_{p'}^N + 3 R_p^{Y_c} \right) \right\} \right\}, \quad (6)$$

$$V_{3D_1}^{Y_c N} = \frac{2}{9} \xi_{Y_c N} \left\{ \left(C_{1S_0} - C'_{1S_0} + 3 C_{3S_1} \right) \left(R_{p'}^N R_p^N - R_{p'}^{Y_c} R_p^{Y_c} \right) \right. \\ \left. + 9 C'_{3S_1} \left[R_{p'}^N R_p^N \left(4 R_{p'}^{Y_c} R_p^{Y_c} - 1 \right) + R_{p'}^{Y_c} R_p^{Y_c} \right] \right\}. \quad (7)$$

where

$$\xi_{Y_c N} = 4\pi \frac{\sqrt{\left(E_{p'}^{Y_c} + M_{Y_c} \right) \left(E_p^{Y_c} + M_{Y_c} \right) \left(E_{p'}^N + M_N \right) \left(E_p^N + M_N \right)}}{4 M_N M_{Y_c}} \quad \text{and} \quad R_{p(p')}^{Y_c, N} = \frac{p(p')}{E_{p(p')}^{Y_c, N} + M_{Y_c, N}}. \quad (8)$$

Note that all the LECs are implicitly pion mass dependent as in Ref. [26] such that $C_{1S_0} = \hat{C}_{1S_0} + D_{1S_0} m_\pi^2$. For M_{Y_c} , we used the average of Λ_c and Σ_c masses. On the other hand, because of the limited LQCD data, it is impossible to pin down all the LECs of the coupled $\Lambda_c N - \Sigma_c N$ system. Therefore, following Ref. [34], we used an effective CT potential by only considering the $\Lambda_c N \rightarrow \Lambda_c N$ channel and assumed that the CT contributions from the $\Sigma_c N$ channel can be effectively absorbed into those from the $\Lambda_c N$ channel, thus in total only four LECs are needed in the present study, i.e. C_{1S_0} , C'_{1S_0} , C_{3S_1} , and C'_{3S_1} .

To construct the OME potentials, we need the following LO meson-baryon Lagrangian [35]:

$$\mathcal{L}_{MB} = \text{tr} \left(\bar{B} (i \not{D} - M_B) B - \frac{D/F}{2} \bar{B} \gamma^\mu \gamma_5 \{ u_\mu, B \}_\pm \right) \\ + \frac{1}{2} \text{tr} (\bar{B}_3 (i \not{\partial} - M_3) B_3) + \text{tr} \frac{1}{8 f_0^2} (i \bar{B}_3 \gamma^\mu \{ [M, \partial_\mu M], B_3 \}) \\ + \text{tr} (\bar{B}_6 (i \not{\partial} - M_6) B_6) + \text{tr} \frac{1}{4 f_0^2} (i \bar{B}_6 \gamma^\mu \{ [M, \partial_\mu M], B_6 \}) \\ + \left(-\frac{1}{\sqrt{2} f_0} \right) g_1 \text{tr} (\bar{B}_6 \gamma^\mu \gamma_5 \partial_\mu M B_6) + \left(-\frac{1}{\sqrt{2} f_0} \right) g_2 \text{tr} (\bar{B}_6 \gamma^\mu \gamma_5 \partial_\mu M B_3) + \text{h.c.} \\ + \left(-\frac{1}{\sqrt{2} f_0} \right) g_6 \text{tr} (\bar{B}_3 \gamma^\mu \gamma_5 \partial_\mu M B_3), \quad (9)$$

where tr indicates trace in the corresponding flavor space, $D_\mu B = \partial_\mu B + [\Gamma_\mu, B]$, Γ_μ and u_μ are the vector and axial vector combinations of the meson fields and their derivatives,

$$\Gamma_\mu = \frac{1}{2} (u^\dagger \partial_\mu u + u \partial_\mu u^\dagger), \quad u_\mu = i (u^\dagger \partial_\mu u - u \partial_\mu u^\dagger).$$

In the Lagrangian \mathcal{L}_{MB} , M_B , M_3 and M_6 are the ground-state masses of octet baryons, antitriplet baryons and sextet baryons,

respectively, and M , B , B_3 , and B_6 refer to the meson and baryon matrices, which are defined as,

$$M = \begin{pmatrix} \frac{\pi^0}{\sqrt{2}} + \frac{\eta}{\sqrt{6}} & \pi^+ & K^+ \\ \pi^- & \frac{-\pi^0}{\sqrt{2}} + \frac{\eta}{\sqrt{6}} & K^0 \\ K^- & \bar{K}^0 & -\frac{2\eta}{\sqrt{6}} \end{pmatrix},$$

$$B = \begin{pmatrix} \frac{\Sigma^0}{\sqrt{2}} + \frac{\Lambda}{\sqrt{6}} & \Sigma^+ & p \\ \Sigma^- & -\frac{\Sigma^0}{\sqrt{2}} + \frac{\Lambda}{\sqrt{6}} & n \\ \Xi^- & \Xi^0 & -\frac{2\Lambda}{\sqrt{6}} \end{pmatrix}, \quad B_3 = \begin{pmatrix} 0 & \Lambda_c^+ & \Xi_c^+ \\ -\Lambda_c^+ & 0 & \Xi_c^0 \\ -\Xi_c^+ & -\Xi_c^0 & 0 \end{pmatrix}, \quad B_6 = \begin{pmatrix} \Sigma_c^{++} & \frac{\Sigma_c^+}{\sqrt{2}} & \frac{\Xi_c'^+}{\sqrt{2}} \\ \frac{\Sigma_c^+}{\sqrt{2}} & \Sigma_c^0 & \frac{\Xi_c'^0}{\sqrt{2}} \\ \frac{\Xi_c'^+}{\sqrt{2}} & \frac{\Xi_c'^0}{\sqrt{2}} & \Omega_0 \end{pmatrix}.$$

The values of the coupling constants g_1 , g_2 , and g_6 , and the meson decay constant f_0 will be specified below. Using \mathcal{L}_{MB} , one can straightforwardly obtain the OME potential,

$$V_{Y_c N \rightarrow Y_c N}^{\text{OME}} = -iN \bar{u}_{Y_c}(p') \left(\frac{\gamma^\mu \gamma_5 q_\mu}{2f_0} \right) u_{Y_c}(p) \frac{i}{\Delta E^2 - q^2 - m^2 + i\epsilon}$$

$$\times \bar{u}_N(-p') \left(\frac{\gamma^\nu \gamma_5 q_\nu}{2f_0} \right) u_N(-p) \times \mathcal{I}_{Y_c N \rightarrow Y_c N}, \quad (10)$$

where $Y_c = \Lambda_c, \Sigma_c$, $q = p' - p$ is the transferred momentum, and m is the mass of the exchanged pseudoscalar meson. Note that we only consider light meson exchanges in the ChEFT. The coupling constant N is defined as,

$$N = g_A^{Y_c Y_c'} g_A^{NN}. \quad (11)$$

Following Ref. [26], $g_A^{Y_c Y_c'}$ and g_A^{NN} are assumed to be pion mass independent and are fixed to be $g_A^{NN} = 1.27$ [36], $g_A^{\Sigma_c \Sigma_c} = 0.71$ [37], and $g_A^{\Lambda_c \Sigma_c} = 0.74$ [37, 38]. On the other hand, the meson decay constant f_0 varies with the pion mass, and the dependence has been deduced, e.g., in Ref. [39]. We use $f_0 = 93$ MeV for $m_\pi = 138$ MeV, $f_0 = 112$ MeV for $m_\pi = 410$ MeV, and $f_0 = 129$ MeV for $m_\pi = 570$ MeV. In Eq. (10), \mathcal{I} indicates the isospin factor, whose value can be found in, e.g., Refs. [40, 41]. Note that OME does not contribute to $\Lambda_c N \rightarrow \Lambda_c N$ at tree level because of isospin conservation, but it contributes to the scattering amplitudes via the scattering equation.

In order to obtain the scattering amplitudes, we solved the coupled-channel Kadyshevsky equation [42],

$$T_{\rho\rho'}^{\nu\nu',J}(p', p; \sqrt{s}) = V_{\rho\rho'}^{\nu\nu',J}(p', p) + \sum_{\rho'', \nu''} \int_0^\infty \frac{dp'' p''^2}{(2\pi)^3} \frac{M_{B_{1,\nu''}} M_{B_{2,\nu''}} V_{\rho\rho''}^{\nu\nu'',J}(p', p'') T_{\rho''\rho'}^{\nu''\nu',J}(p'', p; \sqrt{s})}{E_{1,\nu''} E_{2,\nu''} (\sqrt{s} - E_{1,\nu''} - E_{2,\nu''} + i\epsilon)}, \quad (12)$$

where \sqrt{s} is the total energy of the two-baryon system in the center-of-mass frame and $E_{n,\nu''} = \sqrt{\mathbf{p}''^2 + M_{B_{n,\nu''}}^2}$, ($n = 1, 2$). The labels ν, ν', ν'' denote the particle channels, and ρ, ρ', ρ'' denote the partial waves. In numerical calculations, the potentials in the scattering equation are regularized with an exponential form factor of the following form,

$$f_{\Lambda_F}(p, p') = \exp \left[- \left(\frac{p}{\Lambda_F} \right)^4 - \left(\frac{p'}{\Lambda_F} \right)^4 \right]. \quad (13)$$

More details about the covariant ChEFT can be found in Refs. [5, 29–33].

III. RESULTS AND DISCUSSION

A. Fitted results and extrapolations to the physical point

The four LECs in the CT potential are determined by fitting to the lattice QCD simulations from the HAL QCD Collaboration [25]. For this, we used the $\Lambda_c N$ S -wave phase shifts for $m_\pi = 410$ MeV and 570 MeV with the center-of-mass energy $E_{\text{c.m.}}$ up to 30 MeV. Although the lattice QCD results for $m_\pi = 570$ MeV are probably already beyond the applicability of leading order ChEFT, we included these results in order to pin down the pion mass dependence of the LECs so that we can extrapolate

TABLE I: Baryon masses for different pion masses (in units of MeV) needed in this work [25].

m_π	m_N	m_{Λ_c}	m_{Σ_c}
138	939	2287	2455
412	1215	2434	2575
570	1399	2555	2674

the lattice QCD results to the physical point. In Table I, we list the lattice QCD [25] and physical [36] baryon masses relevant to the present study. Similar to our previous study on the $\Lambda N - \Sigma N$ system [29–31], the fits were first performed with cutoff values in the range of $\Lambda_F = 500 - 750$ MeV. The fitted χ^2 for lattice QCD simulations for different pion masses and the total χ^2 as a function of the cutoff Λ_F are shown in Fig. 2. For the 1S_0 channel, within the cutoff range studied, the $\chi^2/\text{d.o.f.}$ for $m_\pi = 410$ MeV decreases with increasing Λ_F , while the $\chi^2/\text{d.o.f.}$ for $m_\pi = 570$ MeV stays almost constant. On the other hand, for the 3S_1 channel, the $\chi^2/\text{d.o.f.}$ increases with increasing Λ_F for $m_\pi = 570$ MeV, but stabilizes between $\Lambda_F = 550 \sim 700$ MeV for $m_\pi = 410$ MeV. From the right panel, one can see that a cutoff between 500 and 700 MeV yields the minimum χ^2 for all the lattice QCD data fitted. However, since the lattice QCD data for $m_\pi = 570$ MeV were used in our fits, in principle the cutoff value should be larger than the pion mass such that the inclusion of the OME potential is justified. As a result, we choose the range of $\Lambda_F = 600 - 700$ MeV in subsequent analyses, and the fitted LECs are shown in Table II.

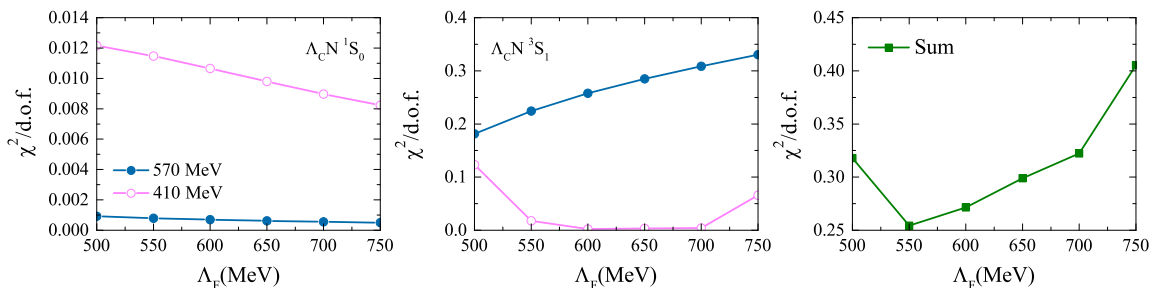


FIG. 2: Best fitted $\chi^2/\text{d.o.f.}$ as a function of the cutoff in the LO covariant ChEFT by fitting to the lattice QCD $\Lambda_c N$ S -wave phase shifts. The magenta circles denote the $\chi^2/\text{d.o.f.}$ for $m_\pi = 410$ MeV, and the dark-blue dots refer to the $\chi^2/\text{d.o.f.}$ for $m_\pi = 570$ MeV, while their sum is shown in the right panel.

TABLE II: Values of the LECs from the best fits obtained with $\Lambda_F = 600 - 700$ MeV, where C'_{1S_0} and C'_{3S_1} are in units of 10^4 GeV^{-2} , and C_{1S_0} and C_{3S_1} are in units of 10^2 GeV^{-2} . The pion mass m_π and cutoff Λ_F are in units of MeV.

m_π	Λ_F	C_{1S_0}	C'_{1S_0}	C_{3S_1}	C'_{3S_1}
410	600	-1.2653	1.6882	0.2698	1.8966
	650	-0.9267	1.8736	0.1270	1.3170
	700	-0.2255	2.1488	-0.0130	0.8456
570	600	-0.7624	0.6540	-0.0520	0.1994
	650	-0.7168	0.6876	-0.0468	0.1608
	700	-0.6485	0.7274	-0.0414	0.1323

The fitted S -wave $\Lambda_c N$ phase shifts are shown in Figs. 3 and 4. For the 1S_0 partial wave, the covariant ChEFT phase shifts are in good agreement with the lattice QCD data. The $\Lambda_c N$ potential turns out to be moderately attractive when extrapolated to the physical point. It should be noted that the predicted 1S_0 phase shifts at the physical point are qualitatively similar to those of the non-relativistic ChEFT of Ref. [26], but with slightly larger uncertainties.

On the other hand, for the 3S_1 partial wave shown in the left panel of Fig. 4, the covariant ChEFT phase shifts are in fair agreement with the lattice QCD data only for energies up to 30 MeV. The discrepancy then becomes larger as the energy increases. Extrapolated to the physical point, the $\Lambda_c N$ interaction is weakly attractive only at the very low energy region then becomes repulsive as the kinetic energy increases. This results in a peculiar phenomenon that although the scattering length of this channel is negative (see Table III) and therefore indicates a weakly attractive interaction, on the whole the 3S_1 interaction is repulsive. This is quite different from the results of the non-relativistic ChEFT [26].

In order to understand this phenomenon, we set $V_{3S_1-3D_1}$ and $V_{3D_1-3S_1}$ in the CT potential to zero, and redid the fits. The

resulting phase shifts are shown in the right panel of Fig. 4. The covariant ChEFT phase shifts are in better agreement with the lattice QCD data for energies up to 40 MeV. In particular, the description of the $m_\pi = 570$ MeV data is much improved. Furthermore, when extrapolated to the physical point, an attractive interaction is obtained, which is similar not only to the 1S_0 interaction shown in Fig. 3, but also to the 3S_1 interaction of the non-relativistic ChEFT. As a result, we conclude that the predicted 3S_1 interaction depends strongly on how the coupled channel $S - D$ mixing is treated.

In the non-relativistic ChEFT, there is no $S - D$ mixing in the leading order CT potential, while the same two LECs are responsible for the $^3S_1 - ^3D_1$ coupled channel in the LO covariant ChEFT. In the following, we further explore this coupled channel effect which is due to relativistic corrections that are considered as of higher order in the non-relativistic ChEFT but already shows up at leading order in the covariant ChEFT.

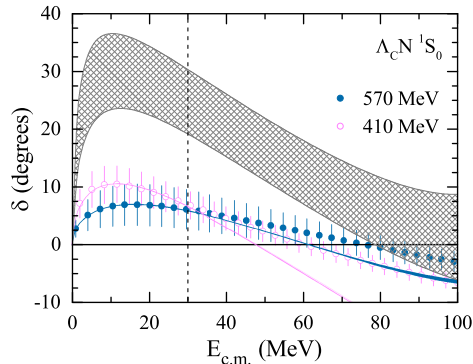


FIG. 3: $\Lambda_c N$ 1S_0 phase shifts of the lattice QCD simulations in comparison with the ChEFT fits. The magenta opened circles denote the LQCD data [25] for $m_\pi = 410$ MeV, while the dark-blue dots refer to the LQCD data [25] for $m_\pi = 570$ MeV. The lines/bands denote the ChEFT fits. The bands are generated from a variation of Λ_F from 600 MeV to 700 MeV. The grey lines/bands refer to the predictions for $m_\pi = 138$ MeV. The vertical dashed lines at $E_{c.m.}$ denote that the $\Lambda_c N$ interaction is obtained by fitting to the lattice QCD data only up to this energy.

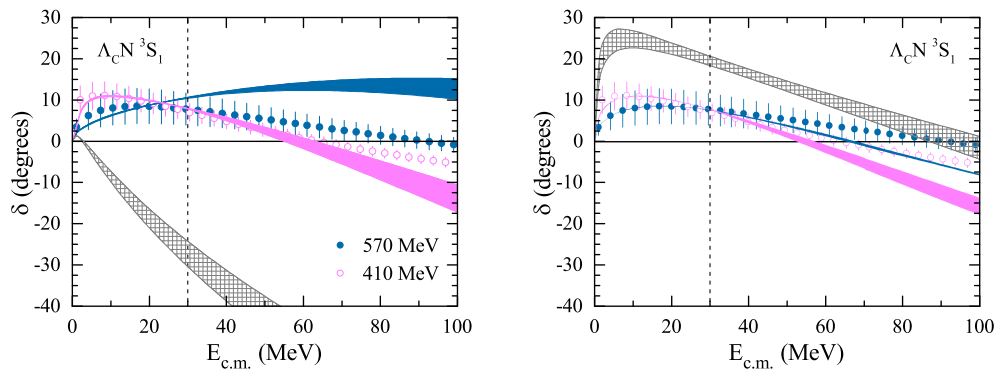


FIG. 4: Left: the same as Fig. 3 but for the 3S_1 phase shifts. Right: the same as the left panel, but with the $S - D$ coupled channel effect turned off. The vertical dashed lines at $E_{c.m.}$ denote that the $\Lambda_c N$ interaction is obtained by fitting to the lattice QCD data only up to this energy.

For the sake of simplicity, we fixed the cutoff Λ_F at 600 MeV, but the general discussion remain unchanged for $\Lambda_F = 650$ and 700 MeV. The on-shell coupled channel potentials as a function of kinetic energy in the center of mass frame are shown in Fig. 5. The 3S_1 potential increases slowly with $E_{c.m.}$, while the 3D_1 and $^3S_1 - ^3D_1$ potentials decrease with the energy. The 3D_1 potential is two order of magnitude smaller than the 3S_1 potential, while the $^3S_1 - ^3D_1$ mixing is even one more order of magnitude smaller. Such features of the triplet channel potentials are in qualitative agreement with the lattice QCD simulations [25]. Nonetheless, the small mixing seems to affect the 3S_1 phase shifts a lot, as we noted above. As a result, we strongly encourage lattice QCD collaborations to check whether the inclusion of the coupled channel effect in extrapolating the 3S_1 interaction can make a difference.

In the following, we predict the 3D_1 phase shifts and the mixing angle ε_1 with the LECs determined by fitting to the lattice QCD 3S_1 phase shifts, which are shown in Fig. 6 together with their 3S_1 counterparts for three pion masses, $m_\pi = 138, 410,$ and 570 MeV. As this is only a leading order study and also demonstrated above, the results beyond $E_{c.m.} > 30$ MeV should be taken with caution. For the 3S_1 partial wave, the interaction changes from weakly attractive to moderately repulsive as the

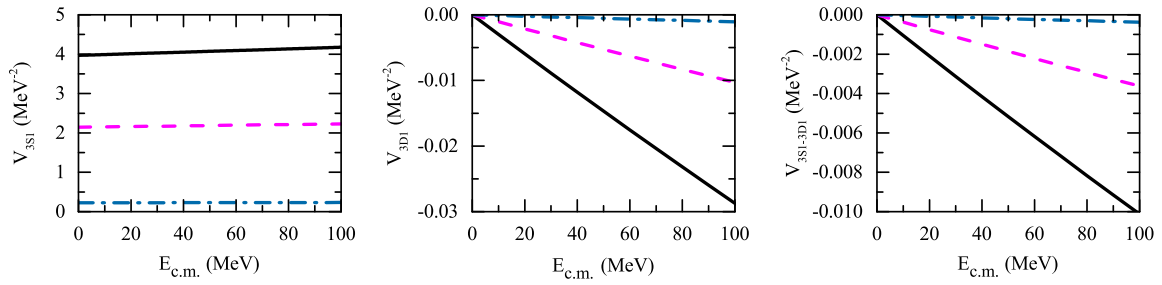


FIG. 5: On-shell $\Lambda_c N$ potentials for the ${}^3S_1 - {}^3D_1$ coupled channel for different pion masses. The black solid lines denote potentials for $m_\pi = 138$ MeV, the magenta dashed lines refer to potentials for $m_\pi = 410$ MeV, and the dark-blue dotted lines are potentials for $m_\pi = 570$ MeV.

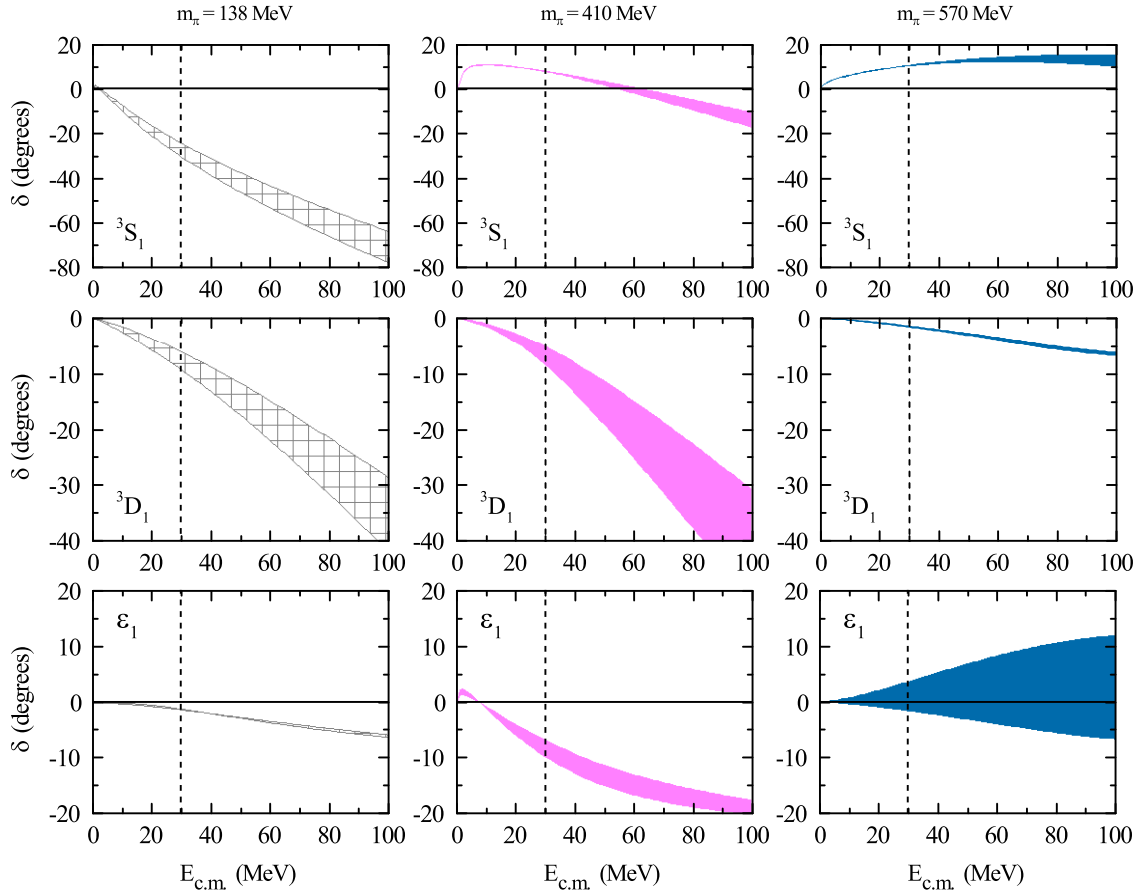


FIG. 6: $\Lambda_c N$ 3S_1 , 3D_1 phase shifts and mixing angles ε_1 for different pion masses. The bands are generated from the variation of Λ_F from 600 MeV to 700 MeV. The vertical dashed lines at $E_{c.m.}$ denote that the $\Lambda_c N$ interaction is obtained by fitting to the lattice QCD data only up to this energy.

pion mass decreases from 570 MeV to 138 MeV. As already stressed above, this transition is strongly related to the $S - D$ coupling and should be checked by future lattice QCD simulations. For the 3D_1 partial wave, the interaction is weakly repulsive for $m_\pi = 570$ MeV, and becomes stronger as the pion mass decreases to $m_\pi = 410$ MeV. However, such a reduction does not extend to the physical point. As a matter of fact, the $\Lambda_c N$ interaction for the physical pion mass is almost the same as that for $m_\pi = 410$ MeV. As for the mixing angle ε_1 , it shows a strong dependence on the cutoff for $m_\pi = 570$ MeV, yet such a dependence becomes weaker as the pion mass decreases. In addition, for $m_\pi = 410$ MeV, the mixing angle has the largest magnitude.

B. Comparison of the NN , ΛN and $\Lambda_c N$ interactions

It is instructive to compare the NN , ΛN and $\Lambda_c N$ interactions, which not only allows for a better understanding of the evolution of the baryon-nucleon interactions as one replaces one light quark in the baryon by one strange or charm quark, but also allows us to better assess the extrapolated $\Lambda_c N$ interaction from the lattice QCD simulations as both the NN and YN interactions are constrained by experimental data, particularly the former.

The 1S_0 and $^3S_1 - ^3D_1$ NN , ΛN and $\Lambda_c N$ phase shifts with $\Lambda_F = 600$ MeV for the physical pion mass are shown in Fig. 7. In the 1S_0 channel, the NN interaction is strongly attractive (to the extent that there is a virtual bound state in this channel), while both the ΛN and $\Lambda_c N$ interactions become less attractive, but the latter two are of similar strength. In the 3S_1 channel, the NN interaction is strongly attractive (to the extent that the deuteron exists), the ΛN interaction becomes only weakly attractive, while the $\Lambda_c N$ interaction becomes weakly repulsive, as we discussed already. In the 3D_1 channel, both the NN and $\Lambda_c N$ interactions are weakly repulsive, while the ΛN interaction is quite small up to $E_{c.m.} \sim 50$ MeV, and then increases quickly, corresponding to the opening of the ΣN channel. Such a phenomenon has been observed in the experimental data [43, 44] and our previous studies [29, 41] that a cusp appears in the $\Lambda p \rightarrow \Lambda p$ cross section at the opening of the $\Sigma^+ n$ channel. On the other hand, the NN and ΛN mixing angles are very similar up to $E_{c.m.} \sim 50$ MeV but the $\Lambda_c N$ mixing angle is negative and smaller in magnitude.

In Table III, we list the corresponding scattering lengths. For comparison, we also show the results of the LO covariant ChEFT [29] for ΛN , next-to-leading order non-relativistic ChEFT [26, 45] for ΛN and $\Lambda_c N$, and Nijmegen-D model [15, 46]. The covariant ChEFT NN scattering lengths were obtained with the regulator of Eq. (13) with a cutoff of 600 MeV following the fitting strategy of Ref. [5] while those of the non-relativistic ChEFT were obtained using the same regulator and cutoff following the fitting strategy of Ref. [47]. We note that the scattering lengths obtained in the covariant ChEFT are qualitatively similar to those obtained in the non-relativistic ChEFT, while some of the predictions of the Nijmegen-D model are drastically different, e.g., those of the $\Lambda_c N$ and 1S_0 NN .

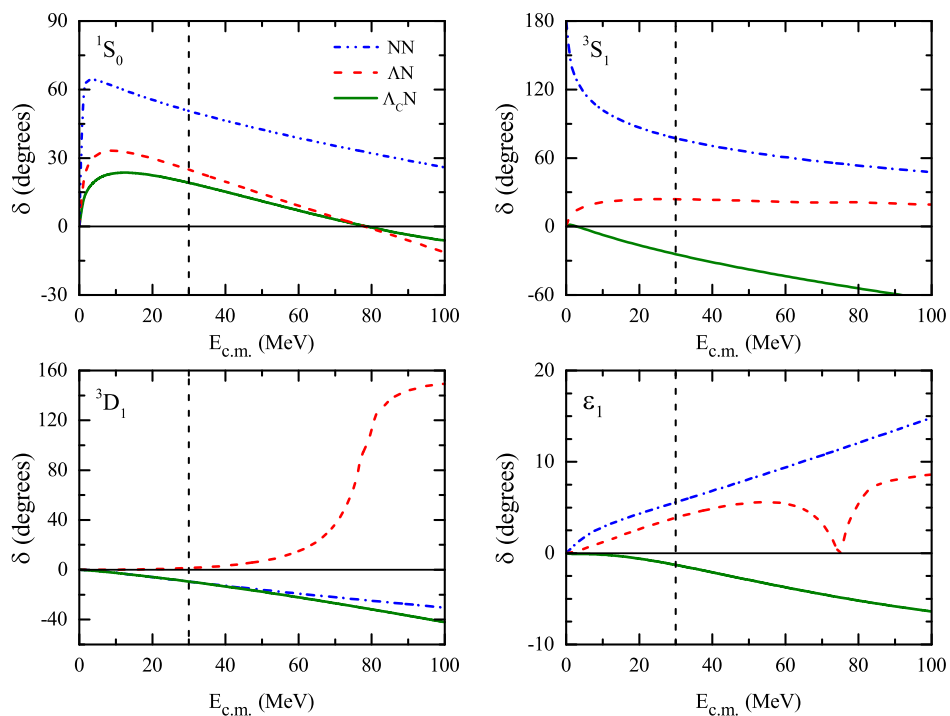


FIG. 7: NN , ΛN and $\Lambda_c N$ phase shifts in the 1S_0 and $^3S_1 - ^3D_1$ coupled channels for physical pion masses. The green solid lines, red dashed lines, and blue dot-dashed lines denote the $\Lambda_c N$, ΛN , and NN interactions, respectively. The vertical dashed lines at $E_{c.m.}$ denote that the $\Lambda_c N$ interaction is obtained by fitting to the lattice QCD data only up to this energy.

IV. CONCLUSION

In this work, we studied the lattice QCD simulations of the $\Lambda_c N$ interaction for $m_\pi = 410, 570$ MeV and extrapolated the results to the physical point. We found that the covariant ChEFT $\Lambda_c N$ phase shifts are in good agreement with the lattice QCD

TABLE III: NN , ΛN and $\Lambda_c N$ scattering lengths (in units of fm) obtained in the LO covariant ChEFT, NLO non-relativistic ChEFT, and Nijmegen-D model. For guidance, we also show the experimental NN scattering lengths.

Channels		Cov. ChEFT (LO)	NR ChEFT (NLO)	Nijmegen-D	Exp.
NN	$a_{1S_0}^{NN}$	-21.3	-23.0	-17.0 [15]	-23.7
	$a_{3S_1}^{NN}$	5.75	5.48	5.42 [15]	5.42
ΛN	$a_{1S_0}^{\Lambda N}$	-2.44 [29]	-2.91 [45]	-1.90 [46]	
	$a_{3S_1}^{\Lambda N}$	-1.32 [29]	-1.54 [45]	-1.96 [46]	
$\Lambda_c N$	$a_{1S_0}^{\Lambda_c N}$	-1.16	-1.00 [26]	-3.83 [15]	
	$a_{3S_1}^{\Lambda_c N}$	-0.52	-0.98 [26]	-4.24 [15]	

simulations in the 1S_0 partial wave for $E_{c.m.} \leq 40$ MeV, while in the 3S_1 partial wave, the ChEFT results are in good agreement with the lattice QCD data for $E_{c.m.} \leq 30$ MeV. Different from the previous study of Ref. [26], we found an attractive $\Lambda_c N$ interaction in the 1S_0 partial wave, but a repulsive interaction in the 3S_1 partial wave, though it is slightly attractive at extremely low energies. We showed that such a repulsive $\Lambda_c N$ interaction is originated from the coupling of 3S_1 and 3D_1 and one ends up with an attractive interaction at the physical point once the coupling in the CT potential is neglected.

To understand how the baryon-nucleon (BN) interaction evolves if one replaces one of the light quarks in the baryon B with a strange or charm quark, We compared the so-obtained $\Lambda_c N$ interaction with those of ΛN and NN . We found that in general the strength of the BN interaction becomes weaker as one moves from NN to ΛN to $\Lambda_c N$.

We noted that although in good agreement with the lattice QCD simulations for unphysical pion masses, the covariant ChEFT results for the spin triplet channel seem to show strong dependence on the consideration of coupled channel effects. This needs to be checked by future and more refined lattice QCD simulations.

V. ACKNOWLEDGEMENTS

This work was partly supported by the National Natural Science Foundation of China (NSFC) under Grants No. 11975041, No.11735003, and No.11961141004. Yang Xiao acknowledges the support from China Scholarship Council.

-
- [1] S. Fleming, T. Mehen and I. W. Stewart, Phys. Rev. C **61**, 044005 (2000)
 - [2] P. F. Bedaque and U. van Kolck, Ann. Rev. Nucl. Part. Sci. **52**, 339 (2002)
 - [3] E. Epelbaum, H. W. Hammer and U. G. Meissner, Rev. Mod. Phys. **81**, 1773 (2009)
 - [4] R. Machleidt and D. R. Entem, Phys. Rept. **503**, 1 (2011)
 - [5] X. L. Ren, K. W. Li, L. S. Geng, B. W. Long, P. Ring and J. Meng, Chin. Phys. C **42**, no. 1, 014103 (2018)
 - [6] C. L. Korpa, A. E. L. Dieperink and R. G. E. Timmermans, Phys. Rev. C **65**, 015208 (2002)
 - [7] J. Haidenbauer, U. G. Meissner, A. Nogga and H. Polinder, Lect. Notes Phys. **724**, 113 (2007)
 - [8] J. Haidenbauer, S. Petschauer, N. Kaiser, U.-G. Meissner, A. Nogga and W. Weise, Nucl. Phys. A **915**, 24 (2013)
 - [9] H. Polinder, J. Haidenbauer and U.-G. Meissner, Phys. Lett. B **653**, 29 (2007)
 - [10] J. Haidenbauer, U. G. Meissner and S. Petschauer, Nucl. Phys. A **954**, 273 (2016)
 - [11] J. Haidenbauer and U.-G. Meissner, Phys. Lett. B **684**, 275 (2010)
 - [12] C. B. Dover and S. H. Kahana, Phys. Rev. Lett. **39**, 1506 (1977).
 - [13] H. Bando and M. Bando, Phys. Lett. **109B**, 164 (1982).
 - [14] H. Bando and S. Nagata, Prog. Theor. Phys. **69**, 557 (1983).
 - [15] B. F. Gibson, G. Bhamathi, C. B. Dover and D. R. Lehman, Phys. Rev. C **27**, 2085 (1983).
 - [16] H. Bando, Prog. Theor. Phys. **81**, 197 (1985).
 - [17] Y. R. Liu and M. Oka, Phys. Rev. D **85**, 014015 (2012)
 - [18] F. Froemel, B. Julia-Diaz and D. O. Riska, Nucl. Phys. A **750**, 337 (2005)
 - [19] S. Maeda, M. Oka, A. Yokota, E. Hiyama and Y. R. Liu, PTEP **2016**, no. 2, 023D02 (2016)
 - [20] S. Nishida, Springer Proc. Phys. **234**, 37 (2019).
 - [21] S. Li [BESIII Collaboration], PoS LeptonPhoton **2019**, 178 (2019).
 - [22] H. Fujioka *et al.*, arXiv:1706.07916 [nucl-ex].
 - [23] T. F. Caramés, C. E. Fontoura, G. Krein, J. Vijande and A. Valcarce, Phys. Rev. D **98**, no. 11, 114019 (2018)
 - [24] [PANDA Collaboration], arXiv:2009.11582 [hep-ex].
 - [25] T. Miyamoto *et al.*, Nucl. Phys. A **971**, 113 (2018)
 - [26] J. Haidenbauer and G. Krein, Eur. Phys. J. A **54** (2018) no.11, 199
 - [27] T. Miyamoto [HAL QCD], PoS Hadron2017, 146 (2018)

- [28] L. Meng, B. Wang and S. L. Zhu, Phys. Rev. C **101**, no. 6, 064002 (2020)
- [29] K. W. Li, X. L. Ren, L. S. Geng and B. W. Long, Chin. Phys. C **42**, no. 1, 014105 (2018)
- [30] J. Song, K. W. Li and L. S. Geng, Phys. Rev. C **97**, no. 6, 065201 (2018)
- [31] K. W. Li, T. Hyodo and L. S. Geng, Phys. Rev. C **98**, no. 6, 065203 (2018)
- [32] X. L. Ren, K. W. Li and L. S. Geng, Nucl. Phys. Rev. **34**, 392 (2017)
- [33] Q. Q. Bai, C. X. Wang, Y. Xiao and L. S. Geng, Phys. Lett. B , 135745 (2020)
- [34] K. Erkelenz, R. Alzetta and K. Holinde, Nucl. Phys. A **176**, 413 (1971).
- [35] T. M. Yan, H. Y. Cheng, C. Y. Cheung, G. L. Lin, Y. C. Lin and H. L. Yu, Phys. Rev. D **46**, 1148 (1992) Erratum: [Phys. Rev. D **55**, 5851 (1997)].
- [36] C. Patrignani *et al.* [Particle Data Group], Chin. Phys. C **40**, no. 10, 100001 (2016).
- [37] K. U. Can, G. Erkol, M. Oka and T. T. Takahashi, Phys. Lett. B **768**, 309 (2017)
- [38] C. Albertus, E. Hernandez, J. Nieves and J. M. Verde-Velasco, Phys. Rev. D **72**, 094022 (2005)
- [39] S. Dürr *et al.* [Budapest-Marseille-Wuppertal Collaboration], Phys. Rev. D **90**, no. 11, 114504 (2014)
- [40] H. Polinder, J. Haidenbauer and U. G. Meissner, Nucl. Phys. A **779**, 244 (2006)
- [41] K. W. Li, X. L. Ren, L. S. Geng and B. Long, Phys. Rev. D **94**, no. 1, 014029 (2016)
- [42] V. G. Kadyshesky, Nucl. Phys. B **6**, 125 (1968).
- [43] J. A. Kadyk, G. Alexander, J. H. Chan, P. Gaposchkin and G. H. Trilling, Nucl. Phys. B **27**, 13 (1971).
- [44] J. M. Hauptman, J. A. Kadyk and G. H. Trilling, Nucl. Phys. B **125**, 29 (1977).
- [45] J. Haidenbauer, U.-G. Meissner and A. Nogga, Eur. Phys. J. A **56**, no. 3, 91 (2020)
- [46] M. M. Nagels, T. A. Rijken and J. J. de Swart, Phys. Rev. D **15**, 2547 (1977).
- [47] E. Epelbaum, W. Gloeckle and U. G. Meissner, Nucl. Phys. A **671**, 295 (2000)